LAWRENCE
LIVERMORE
NATIONAL
LABORATORY

LLNL-TR-852112

Carbon Scaffold Architectures for Stable Lithium Metal Anodes

A. A. Long

July 25, 2023

Disclaimer

This work performed under the auspices of the U.S. Department of Energy by Lawrence Livermore National Laboratory under Contract DE-AC52-07NA27344.

Carbon Scaffold Architectures for Stable Lithium Metal Anodes

Avery Long

Lawrence Livermore National Laboratory

Dr. Marissa Wood

Mentor's Signature: Marissa Wood

Abstract: In light of the skyrocketing demand for electric vehicles and consequent need for high-performing lithium-ion batteries, there has been significant research into the creation of a battery with a lithium metal anode due to its high theoretical capacity and energy density. Unfortunately, nonuniform lithium deposition and consequent dendrite growth diminish performance and pose a safety risk. To combat this, lightweight carbon scaffolds are being developed to stabilize the electric field of these batteries and induce uniform deposition through rational design at the nano-, micro-, and meso- scales. However, there is a paucity of research on the impacts of macroscale scaffold topology on lithium cycling performance. Here, we report the creation of two graphite-based scaffolds with distinct 3D topologies: one a series of triangular prisms and one a series of rectangular prisms. Coin cells were made using these scaffolds and cycled at a current of 1mA/cm^2 for 50 cycles to test the performance. The triangular topology was found to outperform the rectangular topology in terms of both potential magnitude and stability during cycling. Disassembling the cells revealed more even lithium deposition on the rectangular scaffold; however, some of the rectangular prisms were broken while all the triangular prisms remained intact. Last, future experiments are proposed regarding the scaffold spacing and mass of the cells in order to isolate the topological impact.

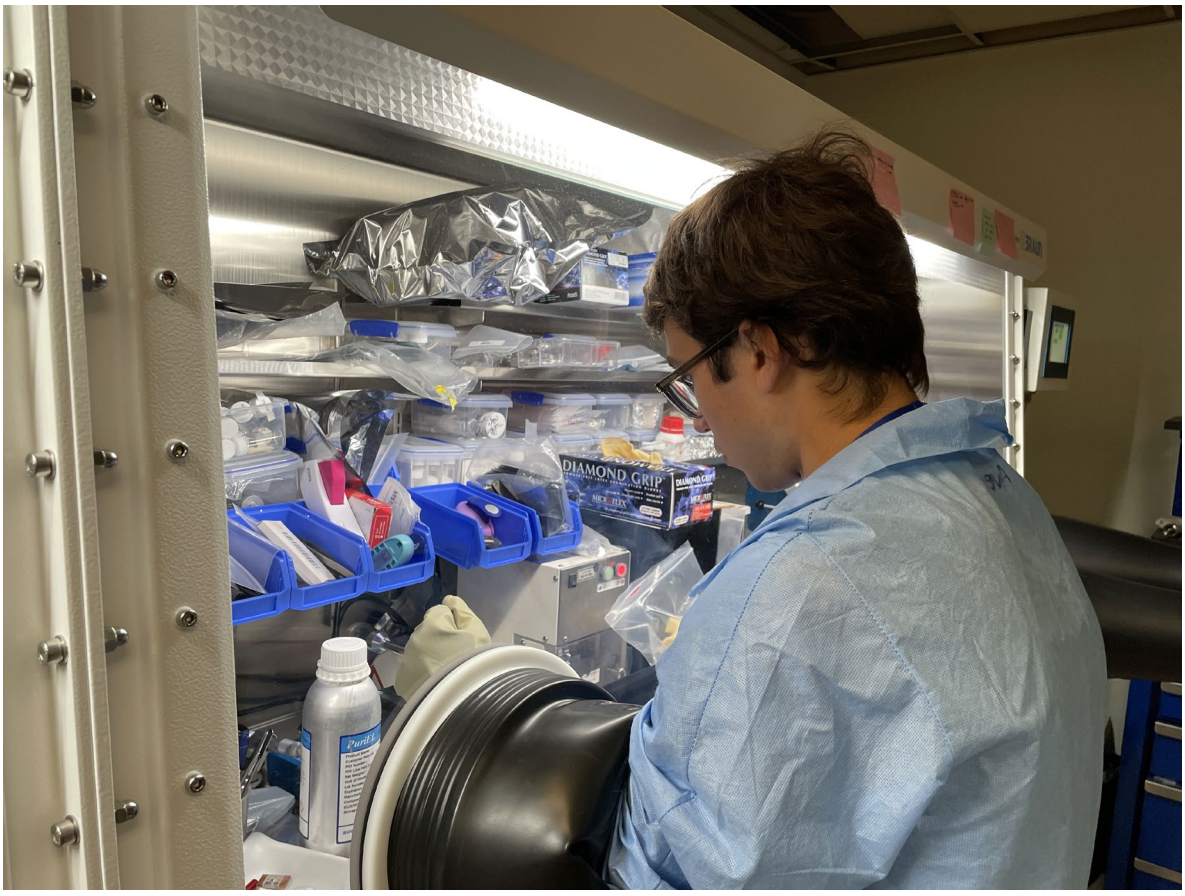

Disassembling coin cells in the glove box. Photo taken by Dr. Marissa Wood

Carbon Scaffold Architectures for Stable Lithium Metal Anodes

Introduction

In response to global climate change and the roughly 21.7% of worldwide greenhouse gas emissions generated by the automotive industry,[1] there is a concerted effort to shift from gas-powered vehicles to electric vehicles (EVs). The most critical components of these vehicles are lithium-ion batteries (LIBs), and electric vehicles comprise over 90% of the LIB demand.[2] Conventional LIBs use graphite anodes, which have a limited storage capacity.[3] The optimal anodic material in terms of battery capacity is lithium (3860 mAh/g compared to 372 mAh/g for graphite), and there is a great deal of research being performed on lithium-metal anodes.[4 5] Unfortunately, there are several practical concerns surrounding the implementation of lithium metal anodes. One of the foremost problems is that lithium metal anodes suffer from dendrite growth upon redeposition of lithium at the anode site.[6 7] These dendrites can break, resulting in the formation of unreactive clumps of "dead-lithium" in the electrolyte that diminish battery performance,[8] or grow to such an extent that they pierce the separator and cause a short—a serious safety hazard at the scale of a car battery.[3 9 10] To combat this problem, research has been conducted on scaffold hosts which stabilize lithium deposition.[11 12] These scaffolds are composed of a variety of materials,[13 14 15 16] the majority of which are carbon-based and feature rationally designed additives and architectures to induce uniform lithium deposition via stabilization of the electric field.[15 17 18] The bulk of this design occurs at micro- or nano-scales; however, there has been little investigation concerning larger topological features. A variety of 3D scaffolds have been presented in the literature,[15 19] but for a given scaffold material there are

no comparisons of how different macroscopic constructions impact lithium deposition. Thus, in this project, we seek to fill this gap in the literature by creating several graphite-based scaffolds with a variety of macroscopic surfaces and shapes in order to determine the impact of topology on scaffold performance.

Description of the Research Project

Project Purpose: In response to a lack of existing literature, the central goal of the project was to examine a series of topological differences in carbon scaffolds to determine if they impact Li anode cycling performance. Specifically, two types of 3D scaffolds featuring rows of consistently spaced rectangular prisms or triangular prisms with roughly equivalent surface areas were fabricated to examine the impacts of 3D shape on scaffold performance.

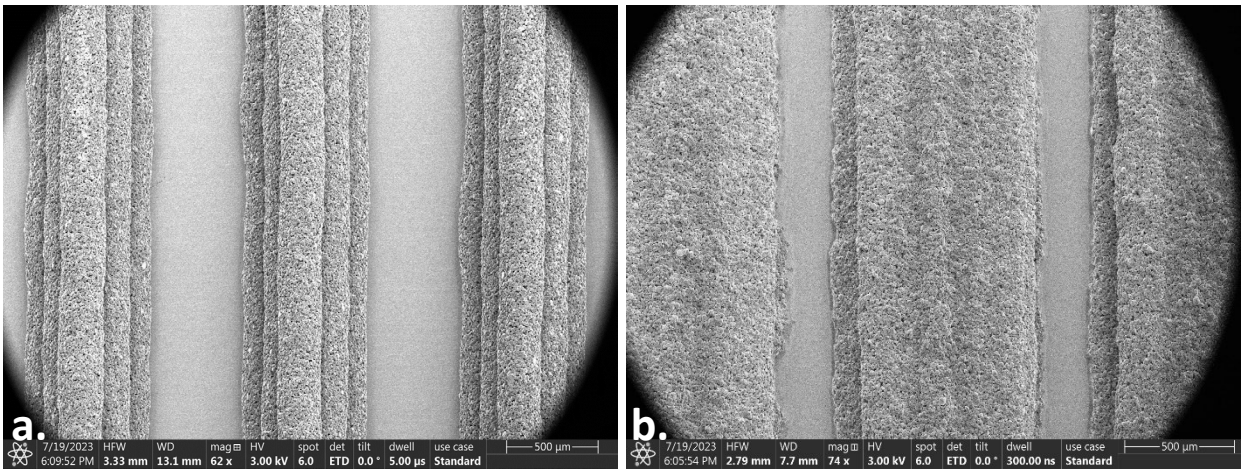

Figure 1. SEM Images of 3D Topologies. The two topologies tested were a series of triangular (1a) and rectangular (1b) prisms.

Materials and Methods

Methodological Overview: In order to control the topology, the scaffolds were created via an extrusion-based 3D printing technique known as direct ink writing (DIW.)[20] A graphite-based slurry was made in house and printed onto a heated copper foil substrate.

Slurry Creation: The slurry was made by alternating between adding components and mixing. All mixing was done in a Thinky AR-100 Conditioning Mixer in the following manner: 60s mixing at 500rpm, 20s mixing at 2000 rpm then 120s defoaming at 2000 rpm, then 30s mixing at 2200 rpm. First, 3g of 3mm yttria stabilized zirconia ceramic beads (Inframat Advanced Materials), 3.9130g of a 10%wt PVDF (Kureha 9300) solution, 0.1073g of N-methyl pyrrolidone (Sigma), and ~3g of graphite (Superior SLC 1520T) were mixed together. Additional graphite was then added such that the total amount was 6g, and the slurry was mixed again. 0.1304g C65 carbon black (MSE Supplies) was added roughly one third at a time, with mixing in between each addition.

Electrode Fabrication: An EnginerHR_Hydra_4_203c printer from Hyrel 3D was used to perform all DIW. The slurry was loaded into a syringe which was fitted with a 0.2 mm nozzle (Nordson) for extrusion. 20mm squares of the desired patterns were printed directly onto 9 μm thick copper foil (MTI) that was heated to 80 ˚C to ensure drying without shape deformation. Once dry, 16mm diameter electrodes were punched out of the foil and dried under vacuum at 115 ˚C overnight.

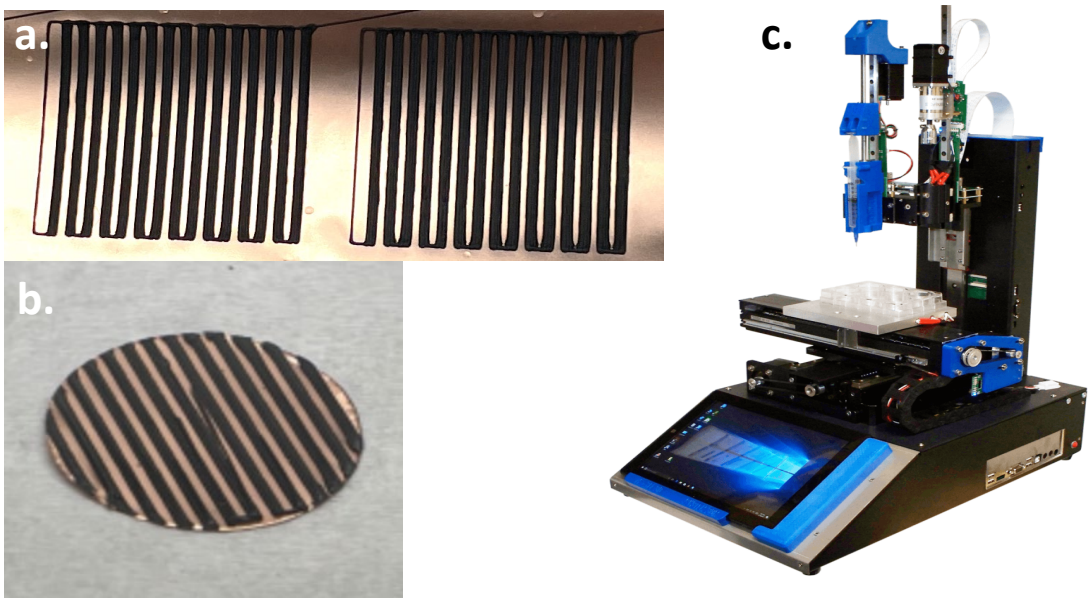

Figure 2. Electrode Preparation. For each of the topological regimes, a series of 20mm square prints were created (2a), from which 16mm diameter electrodes were punched (2b) to be used in coin cell assembly. An EnginerHR_Hydra_4_203c printer (2c) was used to create these prints.

Coin Cell Assembly: Type 2325 coin cells (Hohsen) were assembled in an argon glove box (MBraun) with O_2 and H_2O concentrations <0.5 ppm. The fabricated graphite discs, as well as a plain copper foil disc (control), were used as working electrodes with 16mm diameter lithium discs (MSE Supplies) acting as the counter electrodes. 17mm diameter Celgard 2325 sheets were used as separators, two 16mm stainless steel spacers were used on either side of the electrodes, and 1.2M $LiPF_6$ in 3:7 wt% ethylene carbonate/ethyl methyl carbonate was used as the electrolyte. Each cell contained 8 drops of electrolyte so as to create a flooded cell with electrolyte in excess.

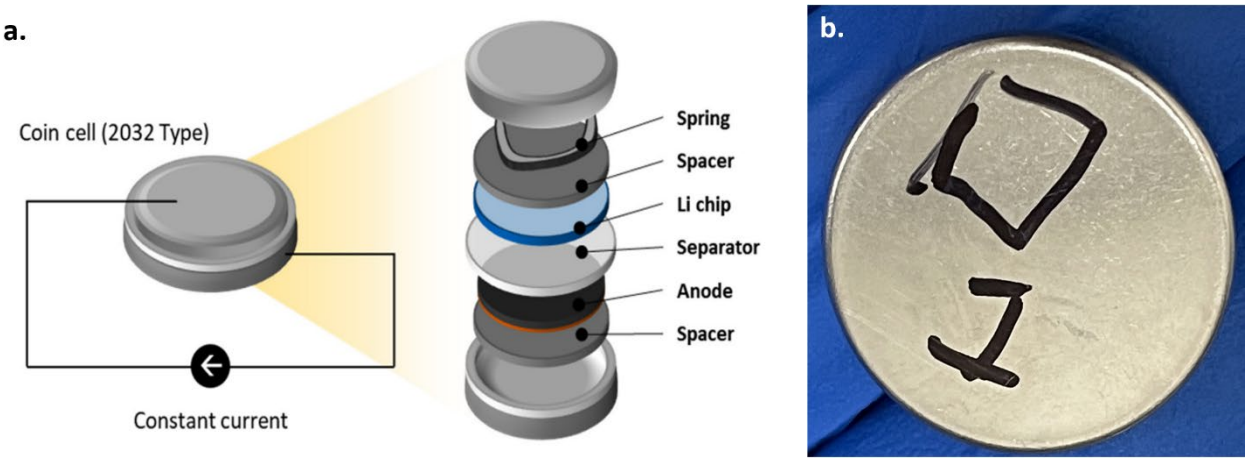

Figure 3. Coin Cell Assembly. To the left (3a) is a diagram of coin cell assembly from *Batteries* 2022, *8,* 14,[21] while the right is a photo of a completed cell (3b).

Electrochemical Testing: All cells underwent three formation cycles at C/10 charge/discharge using a CCCV protocol and a Biologic potentiostat. After formation cycling, the graphite in each cell was fully lithiated, and then Li was plated at 0.5 mA/cm2 for 10 hours to provide an excess Li reservoir. The scaffolds were then cycled at 1 mA/cm^2 at one hour per cycle for 50 cycles.

Results and Discussion

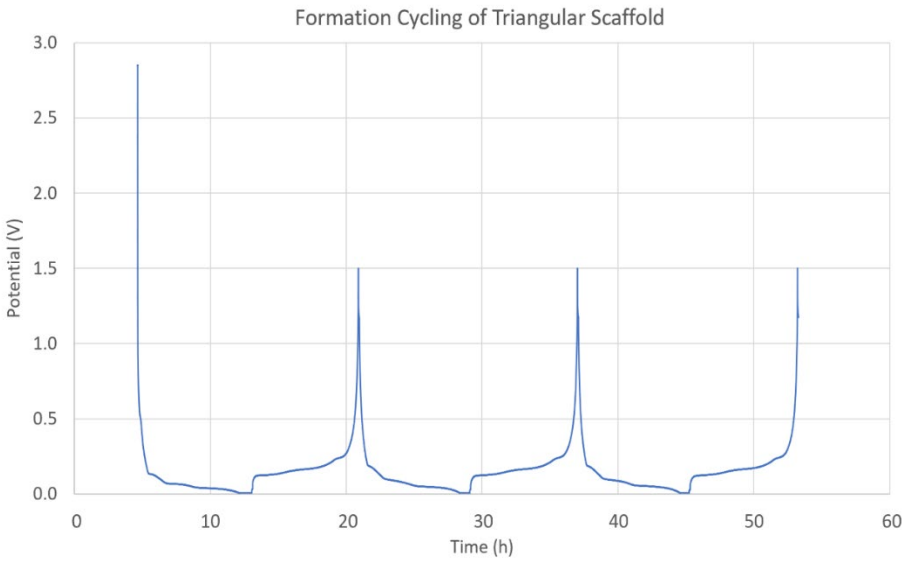

Figure 4. Formation Cycling of the Triangular Scaffold Cell. All cells were cycled at C/10 charge/discharge for three cycles to ensure proper SEI formation.

Before Li cycling, all cells underwent three cycles at low current (C/10) to form a solid-electrolyte interphase (SEI) layer that passivates the surface of the graphite to maximize stability and performance. A representative voltage profile for these formation cycles is shown in Figure 4. The graphite capacity was calculated from the 3rd formation cycle and is shown in Table 1. Although the two had similar surface areas, the overall capacity of the rectangular cell is higher due to the presence of more active material.

	Capacity (mAh)
Triangular Scaffold	7.784
Rectangular Scaffold	15.807

Table 1. Capacities of Cycled Cells. Capacities were obtained from the 3rd formation cycle.

After the formation cycling protocol, the cells were again lithiated at C/10 to ensure that the scaffolds were fully lithiated before beginning the Li plating/stripping testing, as lithium ions preferentially intercalate into the graphite lattice before exhibiting the plating and stripping behavior.[22] Li was then plated and stripped for 50 cycles at a current density of 1 mA/cm^2 (30 min plating; 30 min stripping). A similar test with a current density of 0.5 mA/cm^2 is in progress, but due to time constraints it was not completed by the submitting of this report. 1 mA/cm^2 is a fairly high current density, resulting in fast lithium deposition and stripping processes that are more likely to induce failure than a lower current density. Therefore, differences in scaffold performance at this high current density are more likely to be significant. On the other hand, the milder conditions of lower current densities enable more stringent performance analysis and comparison, hence the additional trial in progress.

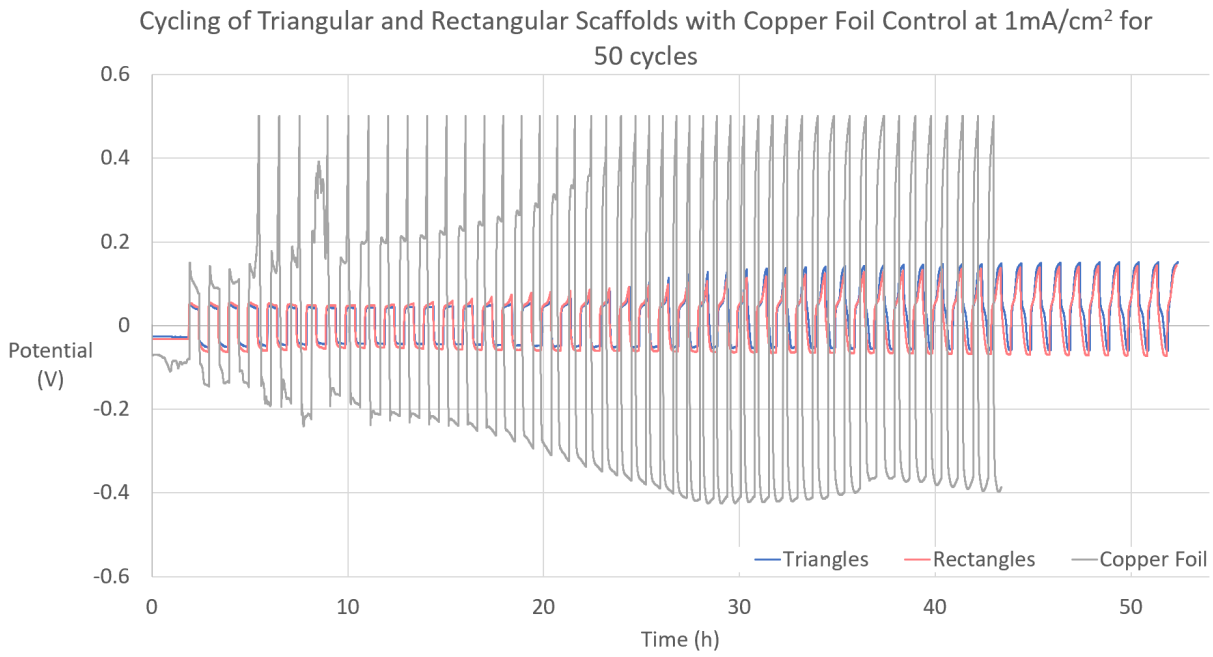

Figure 5. Cycling Data for Tested Cells. The two scaffold cells, along with a control cell containing a bare copper foil electrode, were cycled 50 times at 1mA/cm^2 for a duration of 1h per cycle.

As seen in Figure 5, both scaffold cells start at approximate stripping and plating potentials of 0.05V that drop by cycle 10 and eventually increase to above 0.1V, as plating and stripping becomes less uniform. However, before this point, the cells with triangular scaffolds consistently operate at potentials of lower magnitude than the cells with rectangular scaffolds, suggesting that they are more efficient. With regards to the shape of the cycling data and the consequent constancy of the potential during plating and stripping, the cell with rectangular scaffolds begins to exhibit a sharp peak at the end of the stripping process after 12 cycles, a phenomenon not observed in the triangular counterpart until cycle 16. Additionally, during the stripping process, the initial cycles of both cells have a declining stripping voltage over the half-cycle. The rectangular scaffold cells level off first after 7 cycles; however, this only lasts for 3 cycles. Conversely, though the triangular scaffold cell doesn't fully level off until cycle 10, the overall profile of that cell during stripping from cycles 7-16 is much flatter than the rectangle-based cell,

with cycles 10-14 being almost completely flat. As for plating, the rectangular scaffold cells never have a fully level potential during stable cycling, while the triangular scaffold cells exhibit plating at a flat potential from cycles 12-17. The constant potentials represented by these flat cycles indicate more uniform electric fields in the cell and consequently more uniform plating and stripping behavior, suggesting that the triangular scaffold cells are more stable than the rectangular scaffold cells. Overall, these results indicate that the triangular cells universally outperformed the rectangular cells. Both cells readily outperformed the bare copper foil—the latter exhibited potentials upwards of 0.5V in magnitude and highly inconsistent potentials throughout the cycling steps. This demonstrates the advantage of using a scaffold for Li cycling.

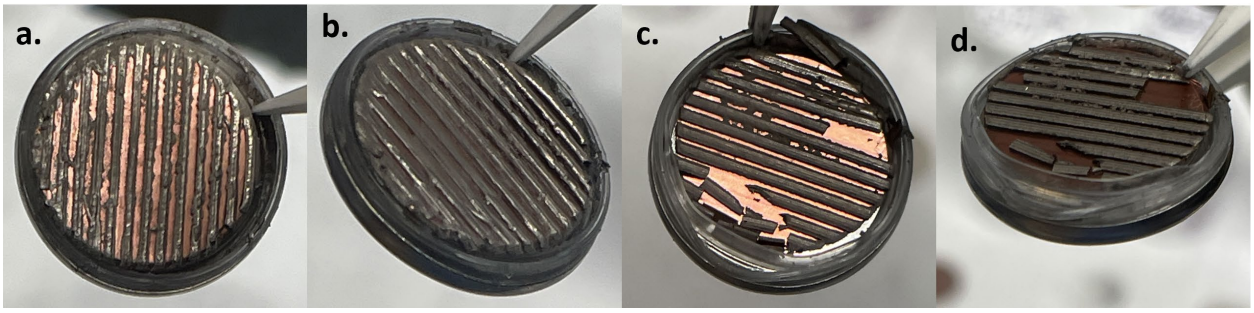

Figure 6. Disassembled Cells Made Using 3D Graphite Scaffolds. After 50 Li plating/stripping cycles at 1 mA/cm2, one cell with triangular prisms (6a and 6b) and one with rectangular prisms (6c and 6d) were disassembled to examine the morphology of lithium deposition.

After cycling the scaffolded cells, they were disassembled to examine the morphology of lithium deposition. Figures 6a and 6b reveal that the triangular prisms largely stayed intact throughout the cycling process, and all had at least some lithium deposition, though it is somewhat uneven. Conversely, as seen in Figures 6c and 6d, the rectangular prisms showed more uniform deposition; however, the scaffolds themselves were less stable on the copper foil, with some pieces detaching. It is difficult to know when the damage to the scaffold occurred, but it is notable that the undamaged components had visibly more uniform lithium deposition despite performing worse in the cycling protocol. In future experimentation, it would be worth

examining whether a scaffold with a similar but more robust rectangular topology would outperform the tested designs.

It is worth noting that there are limitations to the protocol and experimental setup used in this work. Although the surface areas of the two electrode geometries were kept essentially constant, the total mass of the graphite was higher for the rectangular scaffold, which could have had an impact on the performance. Further studies are necessary to determine the effect of mass loading and surface area on Li plating/stripping.

Finally, other inquiries are necessary to completely grasp the effects of topology on scaffold performance. As previously discussed, a less brittle electrode with rectangular topology may outperform the triangular topology. The rectangular electrodes used in this experiment were comprised of two layers of graphite ink. A simple way of testing the topology and improving adherence to the foil would be to replace these with one-layer electrodes. In addition, fabricating and cycling electrodes containing the same 3D prisms with different sized gaps between them would be a simple and effective test of the impacts of spacing. Additionally, mass-based controls are necessary to isolate the impacts of topology—comparing the performance of a given topology across different scaffold masses, and different topologies with roughly equivalent masses would isolate the impact of the shape itself. Last, as previously discussed, additional tests at different current densities will provide further, more nuanced insight into scaffold performance and stability.

Contributions made to the Research Project

I was responsible for most experimental facets of the project: writing Gcode and learning how to use Hyrel's Repetrel software for DIW of the 3D scaffolds, making slurries, printing the 3D

electrodes, and assembling and cycling coin cells, along with performing a significant literature review at the start of the internship while my laboratory access was pending.

What new skills and knowledge did you gain?

I learned a great deal about LIB chemistry, electrochemistry more broadly, and the frontiers of research on lithium metal anodes and using scaffolds to stabilize them. Along the way, I learned how to make electrode slurries, assemble and cycle coin cells, operate a DIW apparatus, and troubleshoot both its mechanical and software issues.

Research Experience Impact on My Academic/Career Planning

Before interning at LLNL this summer, I was fairly confident that I wanted to pursue a career in scientific research but unsure of what setting I would most prefer—academic, industry, government, or something else. I'm happy to say that my experience this summer has reinforced my desire to conduct scientific research, and I'm now strongly considering pursuing further LIB or LIB adjacent research. I'm still not certain on which setting I would most prefer, but I've greatly enjoyed the culture and resources of this lab and am definitely considering national lab work as a result.

Relevance to the Mission of DOE

The stated mission of the DOE is "to ensure America's security and prosperity by addressing its energy, environmental and nuclear challenges through transformative science and technology solutions."[23] Last year over 10 million EVs were sold, comprising 14% of all cars sold worldwide and preventing 13Mt worth of CO_2 emissions—figures projected to dramatically increase in the next decade.[1] Effectively deploying lithium metal anode technology in EV manufacturing would significantly improve EV battery capacity and range. In turn, this

simultaneously furthers the emissions reductions of EVs and makes them more attractive to consumers, resulting in more EVs purchased and further emissions reduced—not to mention the bolstering of the US economy and automobile industry. All of this readily contributes to American security and prosperity, and the cascading benefits demonstrate the multidimensional advantage of investing in science and technology geared toward sustainability.

Acknowledgements

First, I would like to thank my mentor, Dr. Marissa Wood, for her patience and guidance throughout my internship, especially through all of the logistical hurdles at the start. I'd also like to thank Dr. Yiran Xiao and Dr. Jianchao Ye for teaching me how to operate various pieces of necessary equipment and orienting me to the laboratory spaces themselves, as well as Dr. Harry Charalambous for his help in interpreting electrochemical data and making sure my conceptual understanding of LIB chemistry was complete. I'm grateful to ORISE, the EERE AMMTO program, and the DOE for providing me this opportunity, and I'm grateful to LLNL for hosting me this summer. Last, I'd like to thank my fellow interns for their companionship and kindness throughout the summer—I'm honored and privileged to have worked alongside them and gotten to know them as friends.

Lawrence Livermore National Laboratory is operated by Lawrence Livermore National Security, LLC, for the U.S. Department of Energy, National Nuclear Security Administration under Contract DE-AC52-07NA27344

References

1. *CO2 Emissions in 2022*; International Energy Agency: Paris, 2023.
2. Fleischmann, J. H., M.; Horetsky, E.; Ibrahim, D.; Jautelat, S.; Linder, M.; Schaufuss, P.; Torscht, L.; van de Rijt, A. Battery 2030: Resilient, sustainable, and circular. https://www.mckinsey.com/industries/automotive-and-assembly/our-insights/battery-2030-resilient-sustainable-and-circular.
3. Chen, S.; Dai, F.; Cai, M. Opportunities and Challenges of High-Energy Lithium Metal Batteries for Electric Vehicle Applications. *ACS Energy Letters* **2020,** *5* (10), 3140-3151.
4. Wang, R.; Cui, W.; Chu, F.; Wu, F. Lithium metal anodes: Present and future. *Journal of Energy Chemistry* **2020,** *48*, 145-159.
5. Lin, D.; Liu, Y.; Cui, Y. Reviving the lithium metal anode for high-energy batteries. *Nature Nanotechnology* **2017,** *12* (3), 194-206.
6. Wood, K. N.; Kazyak, E.; Chadwick, A. F.; Chen, K.-H.; Zhang, J.-G.; Thornton, K.; Dasgupta, N. P. Dendrites and Pits: Untangling the Complex Behavior of Lithium Metal Anodes through Operando Video Microscopy. *ACS Central Science* **2016,** *2* (11), 790-801.
7. Jana, A.; Ely, D. R.; García, R. E. Dendrite-separator interactions in lithium-based batteries. *Journal of Power Sources* **2015,** *275*, 912-921.
8. Chen, K.-H.; Wood, K. N.; Kazyak, E.; LePage, W. S.; Davis, A. L.; Sanchez, A. J.; Dasgupta, N. P. Dead lithium: mass transport effects on voltage, capacity, and failure of lithium metal anodes. *Journal of Materials Chemistry A* **2017,** *5* (23), 11671-11681.
9. Finegan, D. P.; Darcy, E.; Keyser, M.; Tjaden, B.; Heenan, T. M. M.; Jervis, R.; Bailey, J. J.; Malik, R.; Vo, N. T.; Magdysyuk, O. V.; Atwood, R.; Drakopoulos, M.; DiMichiel, M.; Rack, A.; Hinds, G.; Brett, D. J. L.; Shearing, P. R. Characterising thermal runaway within lithium-ion cells by inducing and monitoring internal short circuits. *Energy & Environmental Science* **2017,** *10* (6), 1377-1388.
10. Yang, C.; Fu, K.; Zhang, Y.; Hitz, E.; Hu, L. Protected Lithium-Metal Anodes in Batteries: From Liquid to Solid. *Advanced Materials* **2017,** *29* (36), 1701169.
11. Shi, P.; Zhang, X.-Q.; Shen, X.; Zhang, R.; Liu, H.; Zhang, Q. A Review of Composite Lithium Metal Anode for Practical Applications. *Advanced Materials Technologies* **2020,** *5* (1), 1900806.
12. Guo, W.; Liu, S.; Guan, X.; Zhang, X.; Liu, X.; Luo, J. Mixed Ion and Electron-Conducting Scaffolds for High-Rate Lithium Metal Anodes. *Advanced Energy Materials* **2019,** *9* (20), 1900193.
13. Zhang, X.; Lv, R.; Wang, A.; Guo, W.; Liu, X.; Luo, J. MXene Aerogel Scaffolds for High-Rate Lithium Metal Anodes. *Angewandte Chemie International Edition* **2018,** *57* (46), 15028-15033.
14. Chen, M.; Zheng, J.; Sheng, O.; Jin, C.; Yuan, H.; Liu, T.; Liu, Y.; Wang, Y.; Nai, J.; Tao, X. Sulfur–nitrogen co-doped porous carbon nanosheets to control lithium growth for a stable lithium metal anode. *Journal of Materials Chemistry A* **2019,** *7* (31), 18267-18274.
15. Jin, C.; Sheng, O.; Luo, J.; Yuan, H.; Fang, C.; Zhang, W.; Huang, H.; Gan, Y.; Xia, Y.; Liang, C.; Zhang, J.; Tao, X. 3D lithium metal embedded within lithiophilic porous matrix for stable lithium metal batteries. *Nano Energy* **2017,** *37*, 177-186.
16. Fang, Y.; Zhang, Y.; Zhu, K.; Lian, R.; Gao, Y.; Yin, J.; Ye, K.; Cheng, K.; Yan, J.; Wang, G.; Wei, Y.; Cao, D. Lithiophilic Three-Dimensional Porous Ti3C2Tx-rGO Membrane as a Stable Scaffold for Safe Alkali Metal (Li or Na) Anodes. *ACS Nano* **2019,** *13* (12), 14319-14328.

17. Nie, X.; Zhang, A.; Liu, Y.; Shen, C.; Chen, M.; Xu, C.; Liu, Q.; Cai, J.; Alfaraidi, A.; Zhou, C. Synthesis of interconnected graphene framework with two-dimensional protective layers for stable lithium metal anodes. *Energy Storage Materials* **2019,** *17*, 341-348.
18. Zhang, A.; Fang, X.; Shen, C.; Liu, Y.; Zhou, C. A carbon nanofiber network for stable lithium metal anodes with high Coulombic efficiency and long cycle life. *Nano Research* **2016,** *9* (11), 3428-3436.
19. Lyu, Z.; Lim, G. J. H.; Guo, R.; Pan, Z.; Zhang, X.; Zhang, H.; He, Z.; Adams, S.; Chen, W.; Ding, J.; Wang, J. 3D-printed electrodes for lithium metal batteries with high areal capacity and high-rate capability. *Energy Storage Materials* **2020,** *24*, 336-342.
20. Saadi, M. A. S. R.; Maguire, A.; Pottackal, N. T.; Thakur, M. S. H.; Ikram, M. M.; Hart, A. J.; Ajayan, P. M.; Rahman, M. M. Direct Ink Writing: A 3D Printing Technology for Diverse Materials. *Advanced Materials* **2022,** *34* (28), 2108855.
21. Möller, S.; Joo, H.; Rasinski, M.; Mann, M.; Figgemeier, E.; Finsterbusch, M. Quantitative Lithiation Depth Profiling in Silicon Containing Anodes Investigated by Ion Beam Analysis. *Batteries* **2022,** *8* (2), 14.
22. Gao, T.; Han, Y.; Fraggedakis, D.; Das, S.; Zhou, T.; Yeh, C.-N.; Xu, S.; Chueh, W. C.; Li, J.; Bazant, M. Z. Interplay of Lithium Intercalation and Plating on a Single Graphite Particle. *Joule* **2021,** *5* (2), 393-414.
23. Mission. DOE, Ed.